Engineering Structures 319 (2024) 118859

Contents lists available at ScienceDirect

Engineering Structures

journal homepage: www.elsevier.com/locate/engstruct

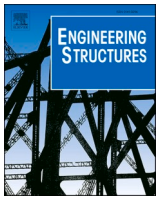

Numerical modelling of global/local mechanisms and sensitivity analysis for the seismic vulnerability assessment of glass curtain walls

Nicola Cella, Chiara Bedon *

University of Trieste, Department of Engineering and Architecture, Via Valerio 6/1, 34127 Trieste, Italy

ARTICLE INFO

Keywords:
Glass Curtain Walls (GCWs)
Earthquakes
Finite Element (FE) numerical modelling
Monotonic response
Cyclic response
Global and local mechanisms

ABSTRACT

Façades represent complex and vulnerable components for buildings, due to the intrinsic fragility and brittleness of glass, and require specific design and calculation tools, both for ordinary and extreme design loads. In this context, the availability of consolidated and strategic modelling strategies is of utmost importance for structural safety considerations and optimal decisions. In this paper, the attention is focused on the assessment of different modelling strategies for the global and local behaviour analysis of Glass Curtain Walls (GCWs) under in-plane seismic loads. Benefits and limitations are discussed for a more refined (but expensive, "MREF") and a simplified (and computationally efficient, but weak in capturing local phenomena, "MSIMP") model assemblies developed in ABAQUS and SAP2000, respectively. Careful consideration is given for typical mechanisms, local responses, key performance indicators for the façade components (i.e., stress and deformation peaks) for a reference GCW under monotonic and cyclic loads, as well as for major effects due to general input parameters (i.e., contact mechanisms, clearance, friction, bare frame features, secondary components, etc.), based on a parametric sensitivity investigation. The parametric comparative results are critically discussed, with the support of an experimental prototype test from literature, and the most influencing parameters are emphasized, to improve and facilitate the development of further design and modelling optimization strategies.

1. Introduction

Glass Curtain Walls (GCWs) are a typical component of modern buildings, providing them a sleek and modern aesthetic. Besides, glass façades are also a well-known criticality for buildings, and require specific design strategies under ordinary and extreme loads. The main reason is represented by the brittle behaviour of glass, which makes these "non-structural" composite systems highly susceptible to damage, and thus a potential hazard for customers life.

According to EN 13830 [1], GCWs consist of vertical and horizontal structural frame elements, usually made of aluminium, connected together and anchored to the load-bearing structure of the building at the floor levels. The light load-bearing framework supports prefabricated infill glass panels, used to form a continuous envelope which guarantees all the basic functions of an external wall. The system can consist of components assembled on site (i.e., stick system) or of pre-assembled interconnected modules (i.e., unitized system). Typically, GCWs are not expected to offer the load-bearing characteristics of the primary building structure, and therefore they are usually classified as "non-structural" elements. Despite this secondary role, however, the behaviour of GCWs subjected to seismic action represents a major threat, since a possible failure is associated to serious risks for occupants and to a major source of economic loss.

In this regard, several surveys conducted after natural earthquakes, as well as extensive laboratory experimental campaigns, highlighted the high vulnerability and susceptibility of CGWs to major damage following large inter-story drifts, even in those buildings that have suffered minimal damage in structural members [2]. This damage is generally due to an intrinsic incompatibility between the deformation of the primary structure and the façade components. As such, there is a major need to develop analysis strategies and technological solutions that are able to optimise the capability of GCWs to satisfy such a huge displacement demand caused by seismic actions.

So far, several research efforts can be found in literature in support of a detailed understanding and/or optimisation of façade mechanisms under earthquakes. Lee et al. [3] numerically addressed the seismic response of curtain walls equipped with displacement control fasteners. The concept is similar to [4], where special control devices were

* Corresponding author.
E-mail address: chiara.bedon@dia.units.it (C. Bedon).

https://doi.org/10.1016/j.engstruct.2024.118859
Received 16 April 2024; Received in revised form 21 July 2024; Accepted 20 August 2024
Available online 24 August 2024

proposed and numerically / analytically addressed for the performance improvement of curtain walls under seismic events. In parallel, full-scale experimental investigations on typical GCW prototypes subjected to in-plane seismic actions were extensively discussed in [5–8], with careful attention for the effect of specific structural features and details under both moderate and severe earthquakes. The parametric experimental investigation reported in [9] for seven different GCW units highlighted the possible failure mechanisms and their sensitivity to design parameters, by considering possible variations in key dimensions and features of components (glass, spandrels and joints). An extensive review on seismic demands and experimental observations was proposed in [10], while considerations and results for fragility curves of curtain walls under seismic events have been elaborated in [11,12]. To support the elaboration of optimal design and seismic vulnerability assessment procedures for GCWs under earthquakes, simple analytical and numerical methods have been also proposed in [13–16].

Actually, the in-plane seismic response of a conventional GCW is in fact a well-known complex mechanism, which involves a combination of geometrical and mechanical features, the multiple interaction of primary and secondary components composed of different materials, the possible propagation of damage mechanisms in materials and components.

According to literature, more in detail, the effect of an imposed inter-story drift on a glass façade can be approximately schematised as shown in Fig. 1, where the deformation of a glass panel within the metal frame is described in three different stages [17,18]:

1. following the in-plane lateral load application / inter-story drift, the glass pane translates rigidly until it makes contact with the frame;
2. the lateral deformation of the frame causes the closure of the glass-frame clearance at two opposite glass corners, and consequently the panel starts rotating;
3. the panel rotates until the two glass corners make contact with those of the surrounding frame.

In the last stage, due to its interaction with the frame, the glass panel acts like a diagonal strut. This final configuration may result in either a compressive crushing failure of glass, or in the falling out of the intact glass panel, due to the progressive loss of supports along the edges.

Currently, from a practical point of view, the available standards do not provide specific guidelines for the evaluation and optimisation of the behaviour of glass façades subject to seismic action. In this regard, two different strategies are generally proposed: the first involves limiting inter-storey drifts [18], while the second aims to provide adequate gaps between glass and frame components, in order to absorb the relative displacements [19]. Therefore, the seismic performance of a façade prototype should be necessarily assessed only through experimental tests on full-scale samples, e.g. according to recommendations provided

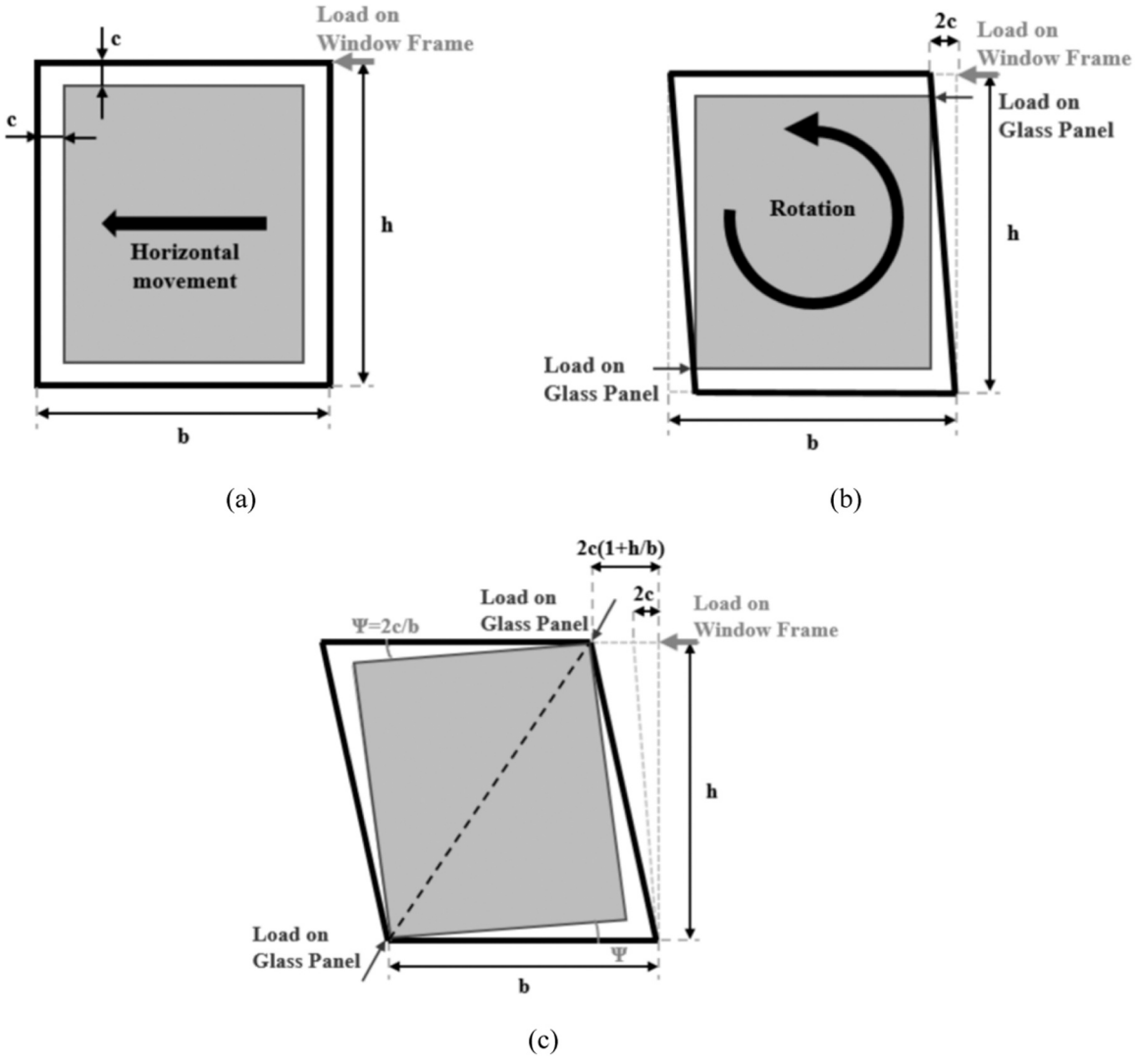

Fig. 1. Typical response of a glass panel under in-plane seismic action [17,18].

by the American Architectural Manufacturers Association (AAMA 501.4–00 [20] and AAMA 501.6–01 [21]). On the other side, the potential and efficiency of FE numerical tools and simulations to minimise the need of complex full-scale experiments is increasingly confirmed and supported by successful applications for the virtual analysis of curtain walls under seismic test protocols [22–26]. In any case, engineering knowledge on the governing parameters and phenomena is still needed for these vulnerable systems.

For this reason, the present study aims to investigate the seismic behaviour of stick systems, to improve the technical knowledge of these systems and assist the development of a reliable modelling strategy that could help minimizing the use of experimental tests. To this aim, a glass façade prototype selected from literature is taken into account, and briefly presented in Section ↱2. Two different modelling strategies – characterised by variations in geometric accuracy and computational efficiency – are described in Section ↱3 for the in-plane seismic performance assessment of the façade. Sections 4 and 5 present a comparison between the collected numerical results and the reference literature experimental data, and a sensitivity parametric analysis to assess the global response of the system under monotonic or cyclic quasi-static in-plane lateral displacements. The latter, in particular, is carried out to identify possible limitations of simplified modelling approaches for the prediction of such a complex mechanical response and interaction of multiple components, which is of utmost importance especially for structural safety purposes under extreme loads. In parallel, the sensitivity study is an efficient way to evaluate and quantify the effect of typical input parameters on the global response (both monotonic and cyclic) of similar glass façades, in order to define a robust modelling

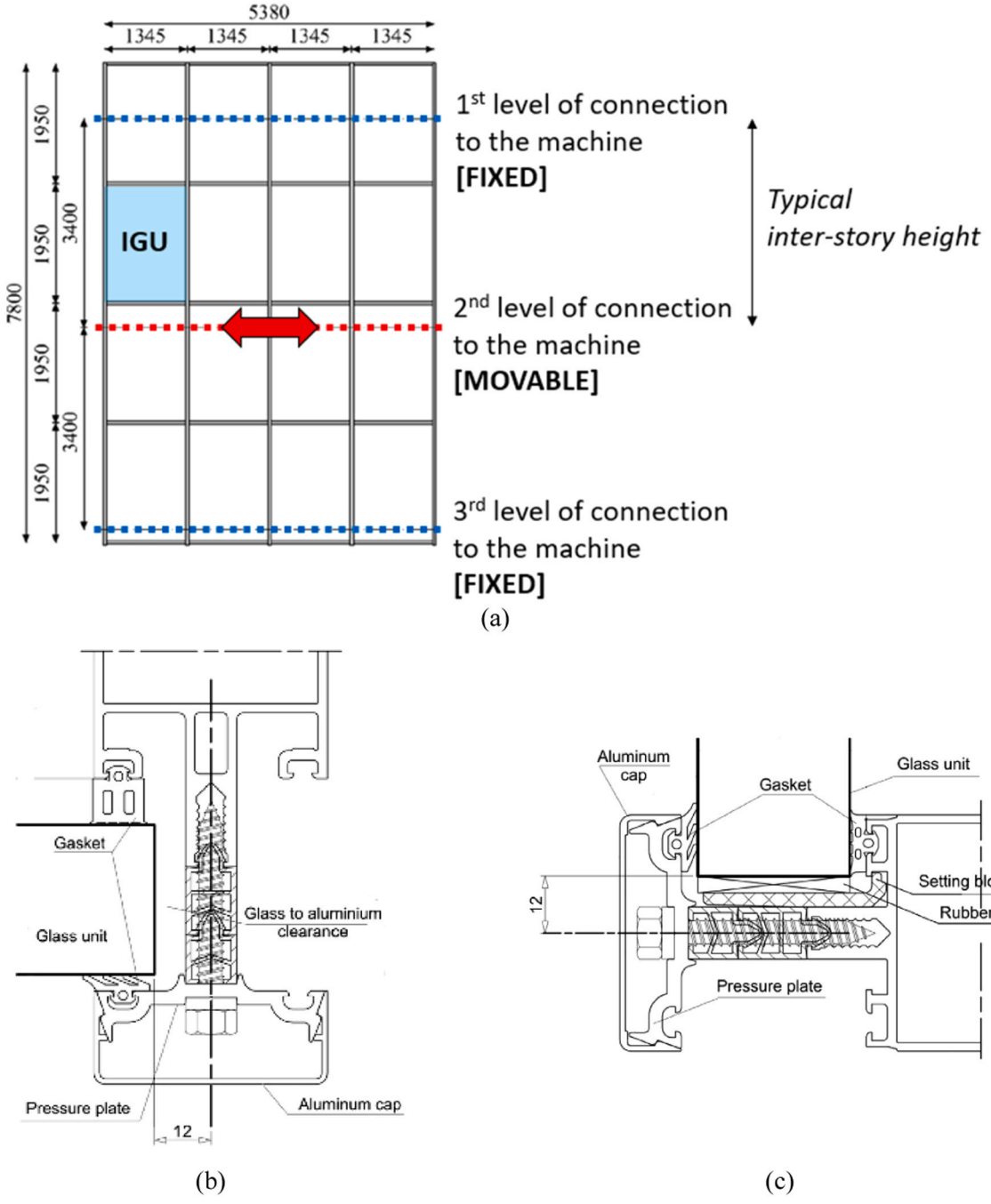

Fig. 2. Reference experimental test [27]: (a) front-view of the GCW, (b) glass-to-mullion and (c) glass-to-transom details (dimensions in mm).

procedure of general validity. Finally, a further comparison of the two numerical assemblies is conducted in Section ↱6 in terms of local performance assessment, with a specific attention to local effects in glass.

2. Case-study GCW

For the present numerical investigation, the typical stick system and the experimental setup presented in [27] was taken into account as a reference. The façade, which is 7.80 m high and 5.38 m wide (Fig. 2(a)), is characterised by a supporting aluminium frame composed of five mullions and twenty transoms, that are mutually connected by U-shaped steel joints.

The glass panels, 1300 mm wide × 1900 mm high, consist of Insulating Glass Units (IGUs) with 44.2/16/44.2 resisting section, in which two laminated layers (composed of two annealed glass panels (4 mm thick) and bonded by means of a polymeric interlayer (two PVB foils with a thickness of 0.38 mm each)) are spaced by a 16 mm cavity. The clearance between the frame and IGUs is 6 mm (Fig. 2(b)). Each IGU is then held in position by means of aluminium pressure plates that are screwed to the frame (Fig. 2(c)). Furthermore, each IGU is supported by two elements that are placed at the ends of transoms, consisting of an aluminium plate (setting blocks) with a layer of plastic material (rubber pads) on top (see Fig. 2(c)).

For the experimental investigation presented in [27], the mullions of the aluminium frame were fixed to the test facility at three different levels, spaced 3.4 m from each other (Fig. 2(a)). This choice was implemented in the experimental setup in order to simulate the effect of a typical inter-story height, as for the façade system rigidly connected to a building and subjected to in-plane seismic actions. The typical façade prototype from [27] was then subjected to a series of eleven in-plane cyclic and dynamic tests, carried out under displacement control.

For the purpose of the present numerical study, only the test "VI" from the series in [27] was taken into account. It consisted in a quasi-static sequence of increasing ramps of horizontal displacement, that were applied to the intermediate movable beam of the test facility (i.e., the 2nd level of connection to the in Fig. 2(a)), with a constant velocity of 1 mm/s. The imposed displacement time-history for the intermediate beam, which reached a maximum of 45 mm (corresponding to approximately ≈1/175 of the façade height), is plotted in Fig. 3. Finally, it is worth noting that glass breakage was not reported in [27] for the selected test.

3. Finite element numerical analysis

Currently, the reference approach to assess the behaviour of a façade subject to seismic action consists in experimental tests on full-scale samples and prototypes like in [27]. This approach – whilst necessary for structural safety purposes – is clearly expensive and time consuming.

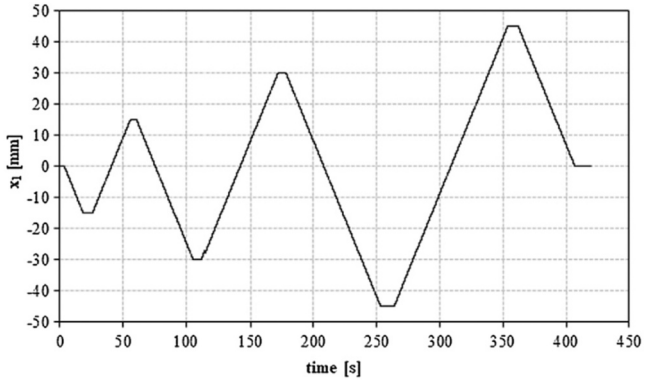

Fig. 3. Imposed horizontal displacement time-history for the reference experimental test [27].

Therefore, it is often preferable to develop a reliable FE numerical strategy to support designers and manufacturers in the optimal detailing and realisation of such systems. On one side, the numerical accuracy is particularly critical, to capture the mechanical interaction of primary and secondary components for a general GCW. On the other side, the need of high computational efficiency suggests major simplifications in the model assembly, which could introduce possible unfavourable mechanisms or lose critical phenomena that are needed for structural safety purposes.

For this reason, two different approaches are discussed in this study to predict the in-plane seismic performance of a stick system. The two strategies differ in terms of geometric accuracy and computational efficiency, with the aim of identifying possible limitations and understanding the degree of approximation of simplified approaches compared to more refined ones. First, a highly refined model is presented in Section ↱3.1.

3.1. Refined model in ABAQUS

A refined micro-model (MREF) of the tested façade was first developed in ABAQUS/Standard [28]. It consisted of three-dimensional solid brick elements (C3D8R type), that were used to accurately reproduce the geometry and interaction of each façade component.

Given the high computational cost required by such an adopted modelling strategy, only 1/4th of the experimental prototype was taken into account for the purpose of the present study, with appropriate boundary conditions to consider the remaining portion of the façade.

More in detail, see Fig. 4(a), the maximum dimension of MREF assembly was determined as 2 × 2 IGUs in width and height, which resulted in 3.9 m high mullions. The 2nd and 3rd level connections to the test machine were numerically reproduced in the form of equivalent nodal restraints. At the same time, a symmetry axis condition – with $U_y = 0$, $UR_y = 0$ and $UR_z = 0$ – was applied at the top section of mullions.

It should be clarified that such an assumption represents a robust approximation that well reproduces the in-plane lateral mechanical response of the investigated façade system, when subjected to the examined setup only, as the horizontally moving beam is located at + 3.4 m rather than at the top mullion section (+3.9 m). This simplification, in particular, was adopted as a trade-off between simplicity and efficiency of modelling, and accuracy of results. To this aim, the symmetry condition strategy as in Fig. 4(a) was properly validated by preliminary simulations carried out on a full-height MREF assembly of the same façade system (i.e., with 2 IGUs in width × 4 in height). The preliminary comparative analysis of the measured in-plane lateral displacements of mullions (at their +3.9 m control section) was quantified in less than 6 % scatter up to the maximum imposed deformation of the system (i.e., 45 mm at the 2nd level connection, in accordance with Fig. 3). For this reason, the 1/4th MREF assembly was used as a reference for further global and local analyses.

Its primary advantage is that in the modelling phase a particular attention was paid also to the description of the various façade components, including the accurate reproduction of IGUs [29,30], as well as to the possible mechanical interactions under the imposed in-plane lateral displacements. In order to facilitate the numerical description and assembly of façade components, and their reciprocal interactions, the geometry of basic elements was only slightly simplified, as it can be seen from the details in Fig. 4(b) and (c).

Regarding the possible mechanical interactions of the façade components under external loads, *surface-to-surface contact* properties with *penalty* and *hard contact* options were defined along all interfaces of IGUs and rubber pads. The *penalty* friction formulation of ABAQUS library is based on the Coulomb's law, and therefore requires the definition of a friction coefficient. As known, this parameter is influenced by many variables and thus its quantification is quite complicated and uncertain. For the present investigation, the friction coefficients shown in Table 1 were iteratively calibrated to obtain the best agreement and fit with the

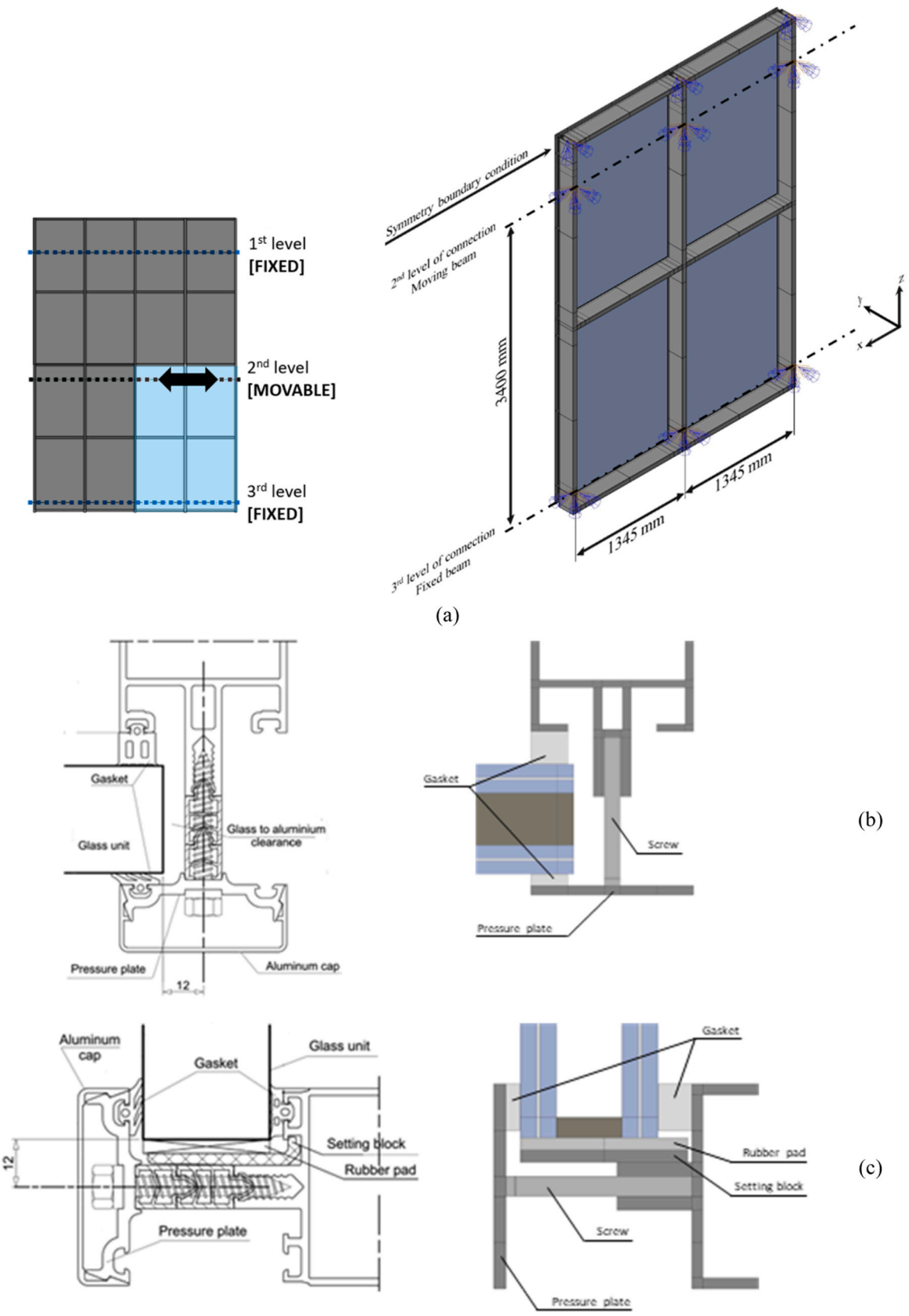

Fig. 4. Refined numerical model in ABAQUS (MREF): (a) 3D-view, (b) glass-to-mullion and (c) glass-to-transom details.

Table 1
Friction coefficients for the refined FE model (MREF).

Surface materials (GCW component)		Friction coefficient
Glass (IGU)	Aluminium (Frame)	0.20
Glass (IGU)	EPDM (Gasket)	0.23
Glass (IGU)	PVB (Rubber pad)	0.20
PVB (Rubber pad)	Aluminium (Setting block)	0.23

reference experimental results.

In relation to the interaction between IGUs and gaskets, it is worth noting that the contact pressure required by the friction formulation was reproduced by applying a −0.6 mm thermal distortion to the screw lengths. For the remaining mechanical interactions, such as frame-gasket and screw-pressure plate, a set of *Tie* constraints was finally used (i.e., null relative displacements and rotations).

The mesh size was defined to avoid distortion of the façade elements, especially the more flexible components affected by severe local deformations under the applied load, with a minimum edge size of 0.3 mm (2.9 mm the average). Such a need resulted in a highly expensive FE assembly. The MREF numerical model corresponding to 1/4th of the façade consisted in fact of about 431,000 solid brick elements and 1510,000 degrees of freedom. Such an approach was chosen to investigate in detail the multitude of possible interactions between components, as well as to assess the role of each component on the global response of the façade.

Regarding the solving approach, based on the experimental protocol described in [27], a dynamic implicit analysis in displacement control was performed. Given the high computational cost of the MREF analysis, the imposed displacement was applied monotonically with the same strain rate of the literature test, until a maximum value of 45 mm (Fig. 3).

3.2. Simplified model in SAP2000

A geometrically simplified and computationally efficient numerical macro-model (MSIMP) – inspired by the modelling strategy discussed in [24] – was also implemented in SAP2000 [31] for the same façade. The model consisted of generic 1D beam elements with nominal section properties, to accurately represent the geometric and mechanical properties of mullions and transoms of the aluminium frame (Fig. 5(a)). According to [27], the latter was assumed to be hinged at both ends. Monolithic 2D shell elements were employed to describe the reference IGUs (with some major simplifications compared to accurate models [29,30]), and their total thickness was set to correspond to the sum of glass layers only (thus disregarding the cavity thickness, the PVB layers and the presence of edge spacer connections). Finally, two different link types available in SAP2000 were used in parallel to qualitatively reproduce the mechanical interaction between the different components of the façade (Fig. 5(b)). In particular:

- "Gap" links were used to represent any contact between IGUs and frame members, following clearance closure (i.e., Fig. 1). To account for the presence and mechanical contribution of setting blocks, the Gap link was set to *Fixed* for all the links introduced in the corresponding region (i.e., glass panels and frame were described as already in contact by means of the setting blocks).
- "Wen" links were used to characterize the mechanical behaviour of gaskets. To avoid the out-of-plane displacement of glass panels, the typical Wen link was set to *Fixed* for the transversal direction.

The link parameters were calibrated as shown in Table 2. It is important to note that the values of such parameters were chosen with the aim of achieving the best agreement between the numerical results and the experimental data, since a reliable local correlation with the façade features is not yet available. Moreover, due to the high computational efficiency of this second modelling strategy, it was possible to describe the entire geometry (4 ×4 IGUs) of the experimental prototype. In doing so, the mesh size of shell elements was defined as a 22 × 22 cm grid, with a local refinement in the region of the setting blocks (Fig. 5 (a)). This choice resulted in about ≈ 1000 shell elements, ≈ 450 frame elements and ≈ 1200 link elements.

To reproduce the experimental test, finally, the reference numerical

Table 2
Calibration of Link parameters.

Link	Gap Link		Wen Link		
	Clearance	Setting block			
Direction	U1	U1	U1	U2	U3
Stiffness [kN/mm]	0.075	Fixed	0.5	0.5	Fixed
Open [mm]	6		-	-	
Post Yield Stiffness Ratio	-		0	0	
Yield Strength [kN]	-		0.05	0.05	
Yielding Exponent	-		1	1	

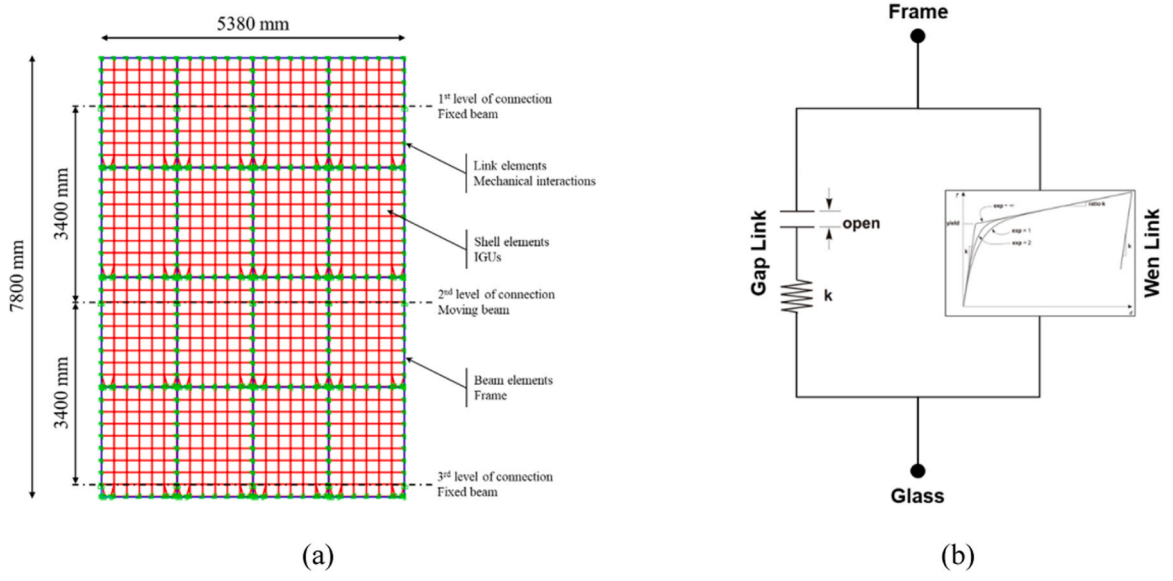

Fig. 5. Simplified numerical model in SAP2000 (MSIMP): (a) front-view and (b) detail of Gap and Wen links.

simulation was defined as a nonlinear Direct-Integration time-history analysis in displacement control. Given the low computational cost of the MSIMP model and its analysis, the imposed displacement was applied both monotonically and in accordance with the cyclic time-history shown in Fig. 3.

3.3. Material properties

The material properties for the MREF components were calibrated as shown in Table 3. It is worth noting that a linear elastic constitutive law was taken into account for most of materials. In this regard, the post-processing stage was carefully focused on the stress peaks evaluation of all façade elements, to ensure the correctness, for the purpose of this study, of the linear elastic material characterisation. Only for aluminium, an elastic-plastic material behaviour with hardening was used, with $f_y = 120MPa$ the yielding stress, $f_u = 160MPa$ the ultimate stress and $\epsilon_{pl} = 0.08$ the corresponding elongation.

It is also interesting to observe that an orthotropic material (i.e., Silicone in Table 3) was used for the spacer connections of the IGUs in order to take into account the spacer bar and the sealant with a simplified approach. Specifically, a Modulus of Elasticity (MoE) of 100 MPa was considered in the direction orthogonal to the glass plane to replicate the stiffness of the spacer bar, while a MoE of 2 MPa was used in-plane to reproduce the behaviour of the sealant. For MSIMP, given the evidence of a linear elastic behaviour obtained by examining the results of MREF, glass and aluminium were both described as linear elastic, with input values from Table 3. For both models, the post-breakage behaviour of glass was not taken into account as no failure occurred during the experimental test.

4. Discussion of numerical results

4.1. Monotonic load-displacement response

Fig. 6 shows the comparison between the experimental response from [27] and the results of the two presently developed FE numerical models. At first sight, thanks to a detailed assembly and robust calibration of MREF and MSIMP models, both the presented models show a good agreement with the experimental curve, and therefore look apparently able to effectively reproduce the global response of the examined façade in terms of load-displacement curve.

Despite the similar recorded path, the MREF and MSIMP models show indeed some local discrepancies in the global load-displacement curve of the system. In detail, the MSIMP assembly results stiffer than the MREF in the initial phase, while it appears less stiff – and consequently less resistant – at the end of the path. In addition, the MSIMP tends to underestimate the expected resistance compared to the experiment and the MREF model, in the range of 5 - 30 mm. Such a result suggests that, despite the final overestimation, the overall best fit of the experimental response is obtained with the refined model developed in ABAQUS. Its final overestimation, which takes place in large displacements only, can be reasonably attributed to the approximate description

Table 3
Material properties.

Material	Density [kg/m^3]	Modulus of Elasticity [MPa]	Poisson's coefficient [-]
Steel	7850	210,000	0.30
Aluminium (6060 T5)	2700	70,000	0.30
Annealed glass	2500	70,000	0.23
PVB	1200	2	0.40
EPDM	1000	2	0.40
Silicone	1400	In-plane: 2 Out-of-plane: 100	0.40

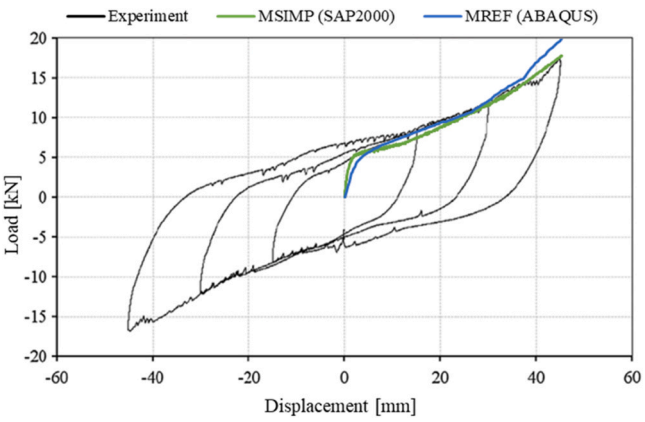

Fig. 6. Monotonic load-displacement response of MREF (ABAQUS) and MSIMP (SAP2000) models, compared to the reference experiment.

of boundary conditions that were introduced – in the 1/4th MREF façade model – to numerically describe the remaining portion of the system and its structural continuity.

The deformed shape of the façade at the maximum imposed displacement, as obtained from the refined ABAQUS model, is shown in Fig. 7. The deformed configuration highlights the typical behaviour of a glass panel within a frame, when subjected to in-plane seismic action, and finds good correlation with the schematic drawing of Fig. 1. In fact, the MREF model shows that each glass panels exhibits an in-plane rotation due to the contact with the frame at two opposite corners. This rotation also causes the detachment of the panel from one of the rubber pads, with the consequent compression of the other rubber pad. In this regard, Fig. 8 shows the evolution of vertical reaction forces for a selected couple of rubber pads, as a function of the imposed in-plane lateral displacement. As shown, the right rubber pad, which is compressed due to the glass panel rotation, reaches a maximum vertical reaction of almost ≈ 2.7 kN, and the reaction force clearly increases with the imposed displacement. On the other side, it can be seen that the glass-rubber pad detachment (i.e., reaction force equal to zero for the left rubber pad) takes place for a rather small imposed lateral displacement, in the order of approximately ≈ 2 mm. This finding suggests that the glass panel rotation begins before any contact of glass with the supporting frame.

4.2. Cyclic load-displacement response

Due to its computational efficiency, the simplified model in SAP2000 was further exploited to investigate the cyclic response of the system. As shown in Fig. 9, the experimental response exhibits an almost symmetrical behaviour, without a significant decrease in stiffness due to subsequent cycles. The good agreement of MSIMP results with the reference test confirms the goodness of the modelling strategy proposed in [24], and further elaborated in [27] for predicting the global seismic behaviour of a traditional stick curtain wall. The calculated scatter between experimental and numerical results are detailed in Table 4, which compares the load-displacement values obtained for each imposed cycle. In terms of measured load, it is interesting to observe the good agreement between the maximum value and the residual one, as recorded at the end of the test. Moreover, the calculated percentage scatter in Table 4 does not exceed the 10 %, which also confirms the stability and accuracy of the model, and its potential for global performance assessment purposes.

Fig. 10 shows the deformed shape of the façade, as obtained in SAP2000 for an imposed displacement of −45 mm. The result in Fig. 10 (b) indicates that the MSIMP assembly is capable of replicating the movement of glass panels within the frame, although there is a significant difference compared to the MREF results. More precisely, the major

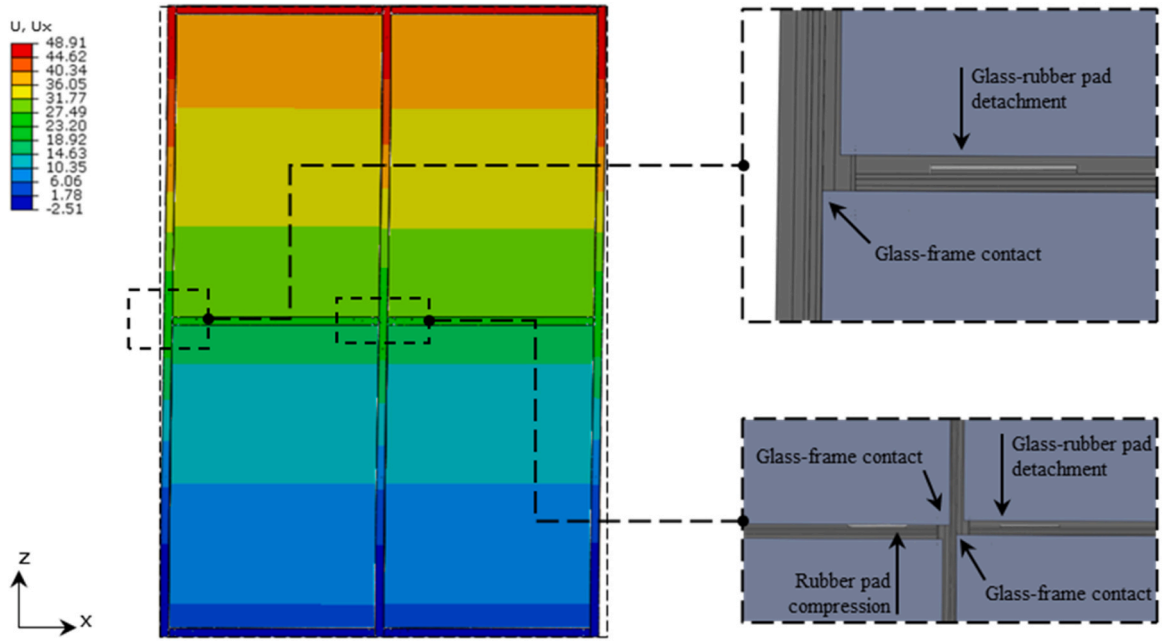

Fig. 7. Deformed shape of the MREF model (ABAQUS) at the maximum imposed displacement of 45 mm (values in mm). Scale factor = 1.

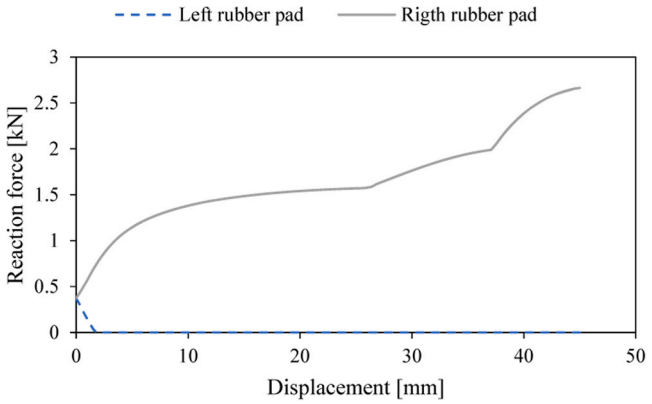

Fig. 8. Typical vertical reaction forces in the rubber pads of the MREF model, as a function of the imposed in-plane lateral displacement (ABAQUS).

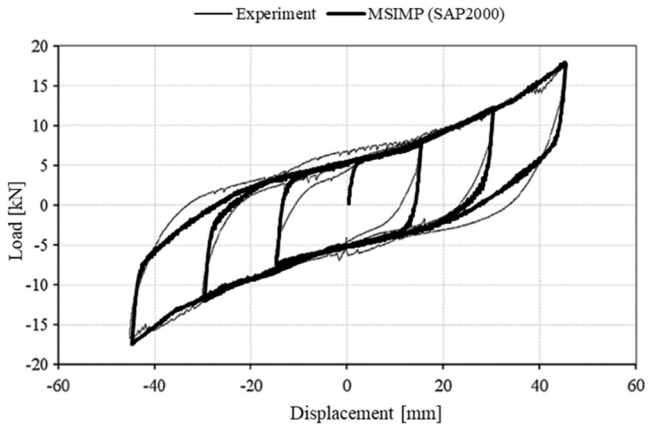

Fig. 9. Cyclic load-displacement response of MSIMP (SAP2000), compared to the reference experiment.

difficulty and limitation of the MSIMP in capturing the mechanical interaction between IGUs and frame members is highlighted in Fig. 11, where the rotation of a reference glass element is shown for both the MREF and MSIMP numerical assemblies. The remarkable discrepancy of comparative results confirms a major limitation of the simplified approach for local assessment purposes, and thus its careful use for structural design considerations.

Table 4
Comparison between experimental and numerical absolute load peaks (MSIMP).

Displacement [mm]	Load [kN]		Difference
	Experimental	Numerical (MSIMP)	
+ 15	7.5	7.4	−1.3 %
−15	7.5	7.5	0.0 %
+ 30	11.5	12.1	+ 5.2 %
−30	11.1	12.2	+ 9.9 %
+ 45	16.1	17.6	+ 9.3 %
−45	17.5	17.5	0.0 %
0	5.2	5.3	1.9 %

5. Sensitivity analysis

5.1. Basic mechanisms and major influencing parameters

The post-processing analysis of parametric results was focused on the detailed analysis of basic mechanisms and major influencing parameters. The present numerical study highlighted – as also in accordance with [24,27] – that the load-displacement response of the examined façade can be schematised in three different branches, as shown in Fig. 12. Moreover, for each branch, the façade response is affected by different parameters/mechanisms.

In detail, the first branch of Fig. 12 (AB) is mainly governed by friction phenomena between the glass panels and the gaskets. Only when the tangential stress at the interface exceeds the critical value (which is defined according to the classical Coulomb formulation), the friction contribution becomes negligible. This means that the behaviour of the façade is successively governed by the in-plane lateral stiffness of the bare aluminium frame, as it can be seen in the branch BC of Fig. 12. Finally, the last branch (CD) is characterised by a moderate stiffness increase for the system, which is due to the contact between the glass panels and the frame. Starting from point C, which ideally corresponds to the first glass-to-frame contact, also the glass panels start to efficiently

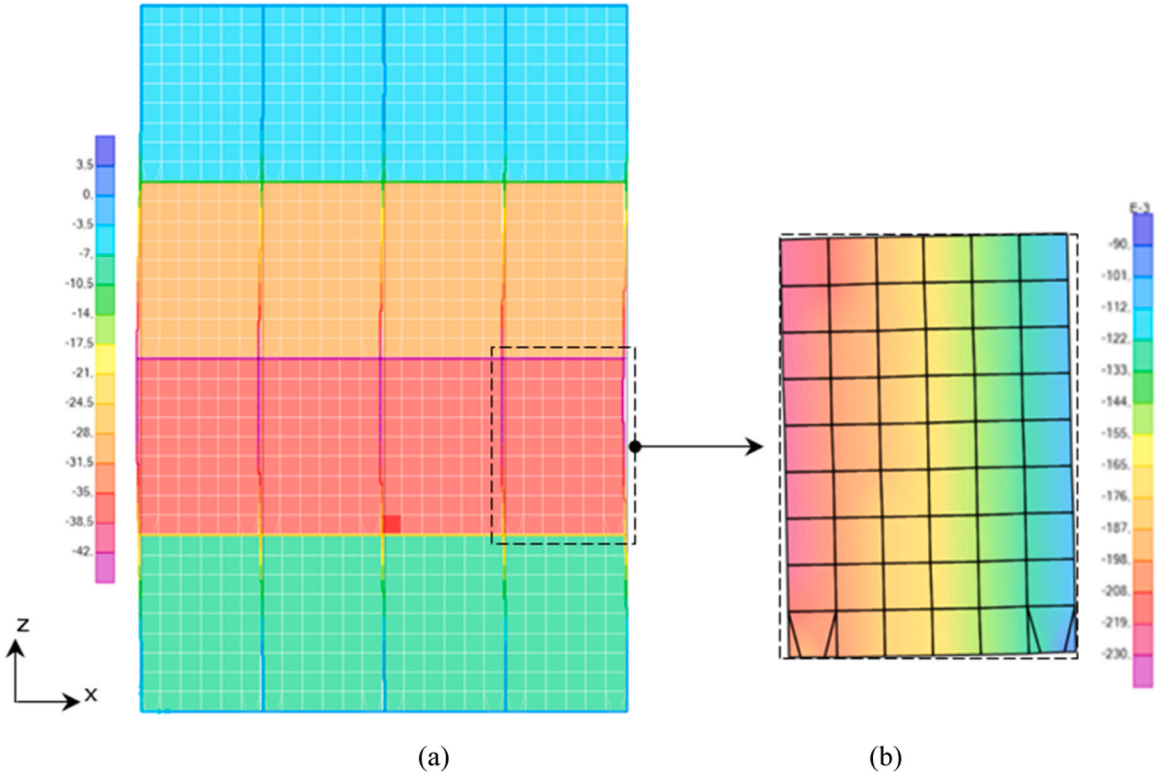

Fig. 10. Deformed shape of the MSIMP model (SAP2000) at the imposed displacement of −45 mm: contour plot of displacement components along (a) x (scale factor = 1) and (b) z (scale factor = 200) directions (values in mm).

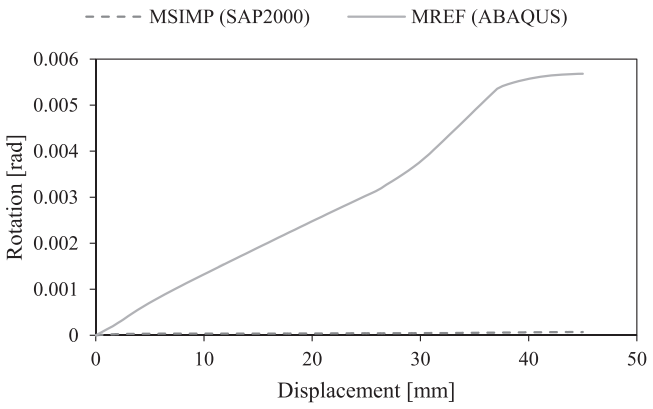

Fig. 11. Rotation of a glass element as a function of the imposed in-plane lateral displacement, as obtained with MREF (ABAQUS) and MSIMP (SAP2000) models.

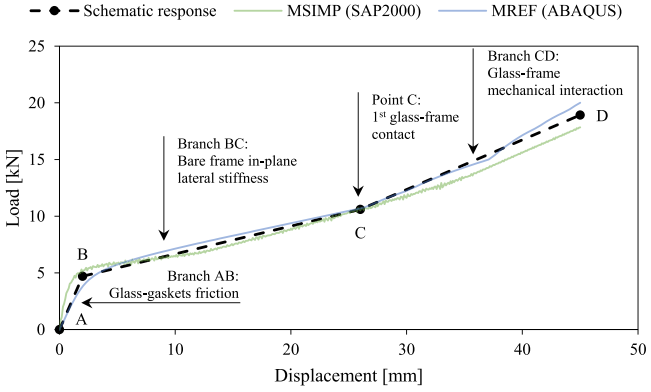

Fig. 12. Schematization of the façade response, with reference branches and key mechanisms.

contribute to the global stiffness of the façade.

In order to identify the principal factors with a relevant effect on the global response of the façade and to possibly quantify their influence, a sensitivity analysis was thus carried out on the two numerical assemblies. In detail, the refined MREF model in ABAQUS was used to evaluate the effect of input parameters on the monotonic load-displacement response of the system, while the cyclic response sensitivity was investigated using the MSIPM assembly in SAP2000. The key input features considered for each analysis are summarised in Table 5.

Table 5
Sensitivity analysis parameters (✓: included; ×: disregarded).

	MREF (ABAQUS)	MSIMP (SAP2000)
Friction between glass and gaskets	✓	✓
In-plane lateral stiffness of the aluminium frame	✓	×
Clearance between glass and frame	✓	✓
Local stiffness in the mechanical interaction between glass and frame	✓	✓
Rubber pad stiffness	✓	×

5.2. Friction between glass and gaskets

The typical response shown in Fig. 12 is initially characterised by a relatively high stiffness for the first branch, which is due to friction between the gaskets and glass. The friction contributes to the façade stiffness until the tangential stress exceeds the critical value and a relative sliding occurs at the interface. Starting from point B in Fig. 12, the stress can be assumed greater than the corresponding critical value and the contribution of glass-gaskets friction to the system response

becomes almost null.

The effect of glass-gasket friction coefficient on the first branch was thus object of sensitivity analyses, as depicted in Fig. 13 (a). Starting from the reference/average value of $\mu = 0.23$ (Table 1), a maximum $\pm$ 10 % deviation was taken into account in the present study, given that gaskets for façades are typically low-friction, soft components required to cushion the glass in the frame and facilitate the relative deformation. From the proposed load-displacement curves of Fig. 13 (a), it can be seen that the increase or decrease of this friction coefficient does not lead to a significant change in the slope of the first branch of the force-displacement curve. Indeed, this change results in a slight and less than proportional variation of the corresponding initial resistance for the façade system, which can be quantified in $\pm$ 5 % for about $\pm$ 8.7 % friction variation (Table 6).

Most importantly, the change in glass-gasket friction does not affect the stiffness of the system after the relative sliding takes place, as also confirmed by the cyclic responses reported in Fig. 13 (b). In this latter case, it should be noted that the effect of friction was taken into account in the MSIMP assembly through the *yield strength* parameter of the Wen link. The latter represents the critical value of friction force that determines the relative sliding of the involved components. For the cyclic load-displacement curves plotted in Fig. 13 (b) – where the friction force is modified up to $\pm$ 50 %, it can be seen that the major effect is a variation in the amount of energy dissipated in each cycle, that can be quantified in up to 275 % for the limit values considered.

Considering that gaskets are typically low-friction components and are used to mitigate the glass elements from severe premature stress peaks, minor effects can be expected in terms of mechanical response of the system.

5.3. In-plane lateral stiffness of the aluminium frame

In the second branch of the reference path, the global in-plane lateral stiffness of the façade system is greatly reduced and its mechanical behaviour is mainly governed by the stiffness of the bare frame alone. The latter, moreover, is strictly dependent on the inter-story height of the façade (i.e., the distance between the three beams of the reference test facility, for the present study).

To qualitatively assess such a complex mechanical interaction, the MREF model was geometrically modified to increase or decrease respectively the reference inter-story height, introducing a $\pm$ 15 % deviation (Table 7).

The effect of the frame stiffness on the global response is shown in Fig. 14, in which the load-displacement response is reported for different inter-story heights. It is evident that the frame stiffness is the parameter with major influence on the second branch, and the measured slope is more than inversely proportional to the inter-storey height of the system.

It is also worth to note that the same parameter is mostly negligible for the first branch of Fig. 14, which further confirms that the glass-gaskets friction is the most influential parameter for the initial phase of the global response.

Table 6
Effect of glass-gasket friction.

Input property	Input value	Variation	Major observed effect	
Friction coefficient	0.23	0.25 (+8.7 %) 0.21 (−8.7 %)	Initial strength	+ 5 % −5 %

5.4. Clearance between glass and frame

The last section of the load-displacement curve schematically shown in Fig. 12 presents a further increase in the global stiffness of the façade, due to the contact initiation between glass and frame components. Among other geometrical features, the amplitude of the imposed in-plane lateral displacement that determines this contact strictly depends on the clearance between them. The different gaps considered in the present parametric analysis are shown in Fig. 15 and Table 8.

The effect of clearance on both the monotonic and cyclic response of the system is depicted in Fig. 16 (a) and (b), respectively. As expected, the minimization of this gap amplitude results in the anticipated contact of glass and aluminium components (i.e., for a smaller imposed in-plane lateral displacement). It is also interesting to observe that the three numerical load-displacement curves of Fig. 16 are identical, until the first contact between glass and frame occurs. At the same time, it is worth noting that decreasing the glass-frame distance leads to a significant change in the mechanical response of the façade, with a maximum strength increase up to $\approx$ 85 % for the configuration with minimum clearance.

Regarding the cyclic response in Fig. 16 (b), an increase in maximum strength (very similar to the monotonic curves) can be observed by changing the *open* parameter of the Gap link for the MSIMP assembly. However, compared to MREF, it can be seen that the recorded residual value at the end of the cycle is not affected by the clearance change, in

Table 7
Effect of inter-story height.

Input property	Input value	Variation	Major observed effect	
Inter-story height	3400 mm	3900 mm (+15 %) 2860 mm (−15 %)	Second branch stiffness	−21 % + 48 %

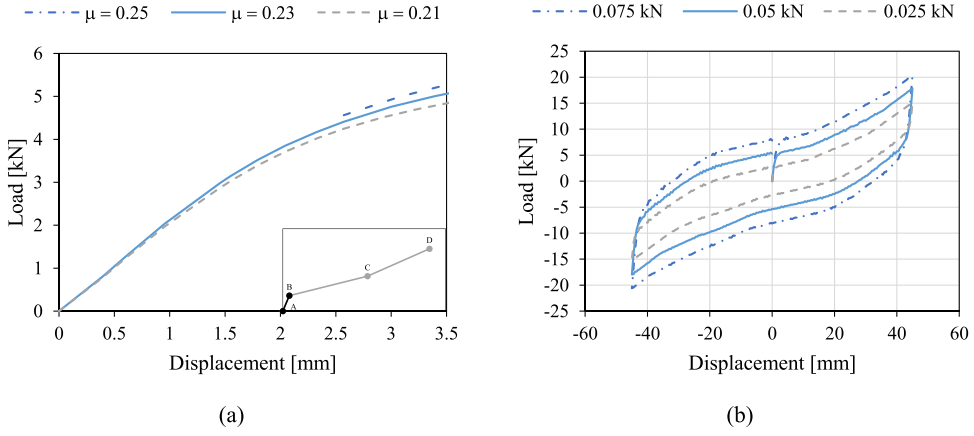

(a) (b)

Fig. 13. Effect of glass-gaskets friction: (a) monotonic (MREF) and (b) cyclic (MSIMP) load-displacement responses.

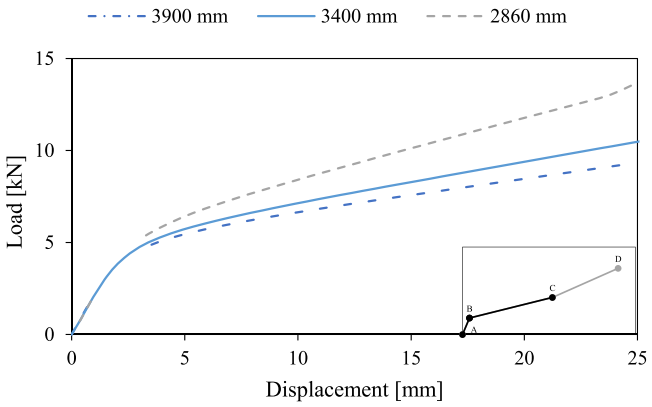

Fig. 14. Effect of bare frame in-plane lateral stiffness on the monotonic load-displacement response (MREF).

the same way of the energy dissipated by the cycle. Also in this case, such a global effect could be justified by the poor mechanical interaction of glass and frame components, that the MSIMP assembly cannot be efficiently captured like for MREF.

5.5. Local stiffness and mechanical interaction between glass and frame

The effect of the glass and frame local stiffnesses on the third branch (CD) of the reference load-displacement response was successively considered. Under the progressive displacement and rotation of glass components in a global mechanisms like Fig. 1, the aluminium mullion that are directly in contact with IGUs are in fact affected by a local deformation in compression, which is a function of the component geometry and the material mechanical properties. In this specific stage of the façade response, due to the relative position of glass panels (see the schematic model of Fig. 1)), the contact is strongly asymmetrical and – as the local deformation of the aluminium frame increases – it is localised at the inner edge of IGU. This typical behaviour is emphasised in Fig. 17, where the contact region for glass (top inner edge) is shown as a function of two different amplitudes of imposed displacement, in terms of contact pressures (CPRESS) exerted by the lateral surface of mullion.

By taking into account the above considerations, the effect of local frame stiffness on the MREF global response was investigated by locally varying the MoE assigned to the mullion wall (see the cross-section detail of Fig. 18 and Table 9). The material properties were in fact modified for a reduced set of brick elements (i.e., mullion wall in the region of model directly involved in the contact mechanism), rather than for the entire components.

More in detail, a fictious aluminium MoE corresponding to weak (−99 %) or ideally rigid (+200 %) local contact was taken into account for the mullion wall. In parallel, the effect of local stiffness on the side of glass was also taken into account, by changing the in-plane MoE assigned to the interposed Silicone material (Tables 3 and 9). In this second case, the fictious MoE of soft Silicone was modified to equal glass/aluminium, or even doubled.

Table 8
Effect of glass-frame clearance.

Input property	Input value	Variation	Major observed effect	
Clearance	6 mm	4 mm (−33.3 %)	Contact displacement	−26 %
		8 mm (+33.3 %)		+ 23 %

The effect of both frame and glass local stiffnesses is shown in Table 9 and Fig. 19 (a) and (b), respectively. It can be noted that for both the considered parameters, any change of the examined MoE values leads to a negligible variation in terms of global stiffness and resistance of the façade, in particular for the final branch (CD) of the load-displacement response, where the glass-frame contact is crucial.

The local stiffness of mullion walls minimally impacts on the predicted maximum load (less than 5 % variation with an ideally rigid wall, see Table 9 and Fig. 19 (a)). The local effect of the silicon bad on this contact interaction is even less pronounced (Table 9 and Fig. 19 (b)). As such, it can be concluded that this local effect does not significantly influence the mechanical interaction of glass and frame components under monotonic loading, and the resulting global response under in-plane lateral loads.

In the MSIMP assembly, the effect of local stiffness in the glass-frame contact mechanisms was also properly considered. In this case, however, such a variation was taken into account in terms of *stiffness* parameter for the description of the Gap link. In contrast to the MREF monotonic response, the cyclic load-displacement curves in Fig. 20 show a relevant increase in the maximum load sustained by the façade, which is approximately linearly proportional to the Gap stiffness increase (up to +24 % load increase when the local stiffness increases +33.3 %). However, even in this case, the energy dissipated in the typical cycle, and the residual value of load, exhibit a negligible variation, which was measured in less than 1 %.

5.6. Rubber pad stiffness

Finally, the role of rubber pads was also investigated. These “soft” elements play a mechanical role of primary importance for the façade as a whole, since they are expected to facilitate the interaction of glass panels with the frame, preventing any premature stress peak and failure of glass. For this reason, rubber pads are typically subject to high reaction forces when the façade is subjected to seismic actions.

In the present study, the effect of rubber pad stiffness was addressed by considering increase MoE values for their mechanical characterisation (Table 10).

The increase of MoE for the rubber pads, as shown in Fig. 21, was

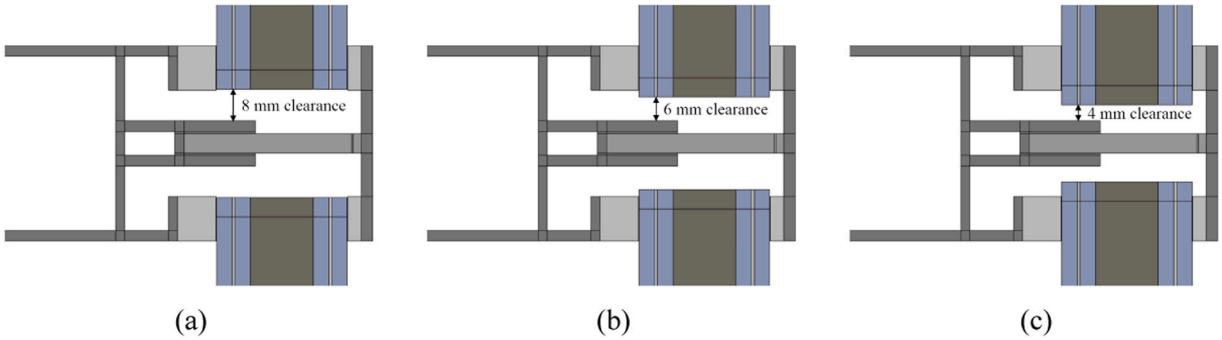

Fig. 15. Glass-frame clearance amplitudes taken into account in the sensitivity analysis.

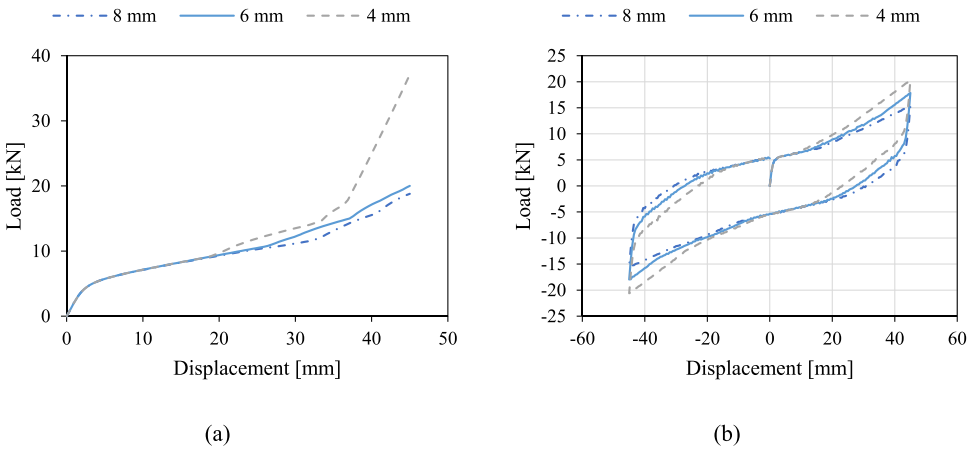

Fig. 16. Effect of glass-frame clearance: (a) monotonic (MREF) and (b) cyclic (MSIMP) load-displacement responses.

observed associated to two different effects. First, a locally augmented stiffness leads to an increase of the in-plane lateral stiffness of the façade that can be estimated up to + 43 % for the first branch of the path. This is not the case of the second branch, which results mostly unaffected by this input variation. The effect of rubber pad MoE is again evident in the final branch of the load-displacement curve, which shows an increase of in-plane lateral stiffness for a lower imposed displacement, as the MoE increases. Such a mechanism was found associated to a moderate final strength increase for the system (up to +29 % when rubber pads are stiff, see Table 10).

5.7. Summary of parametric results

In conclusion, Table 11 summarizes the parameters considered for the sensitivity analysis, and their corresponding major effect on the load-displacement response of the façade system.

The obtained results, as shown, confirm the fundamental role of the aluminium frame and in particular its lateral stiffness, as well as the glass-frame clearance and the rubber pad stiffness, in defining the global in-plane lateral response of similar façades. In particular, the relevant impact of rubber pads highlights the key role of "secondary" components, and further confirms the complexity of this type of systems, as well as the need of refined computational strategies for an accurate modelling and structural design procedure. This effect is further quantified by the sensitivity measure in Table 11, which accounts for the

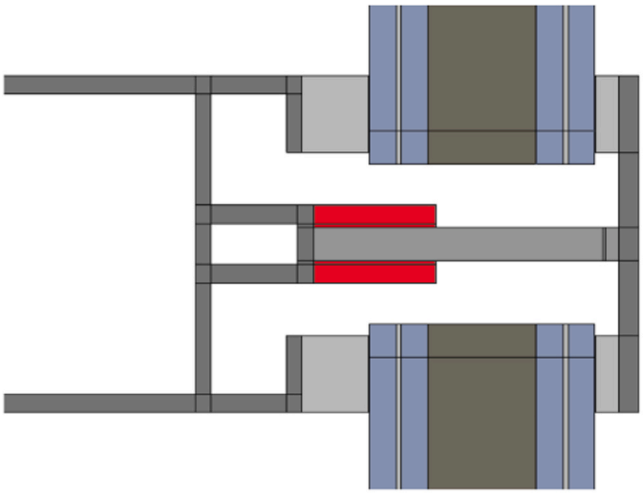

Fig. 18. Aluminium mullion wall (in red) in contact with the glass panel, under the applied in-plane lateral displacement (ABAQUS).

observed phenomena and expected impact of the considered parameters. In consideration of these evidences, further experimental studies are necessarily needed to evaluate the effect of different types of rubber pads and setting blocks to accommodate the movement of glass panels

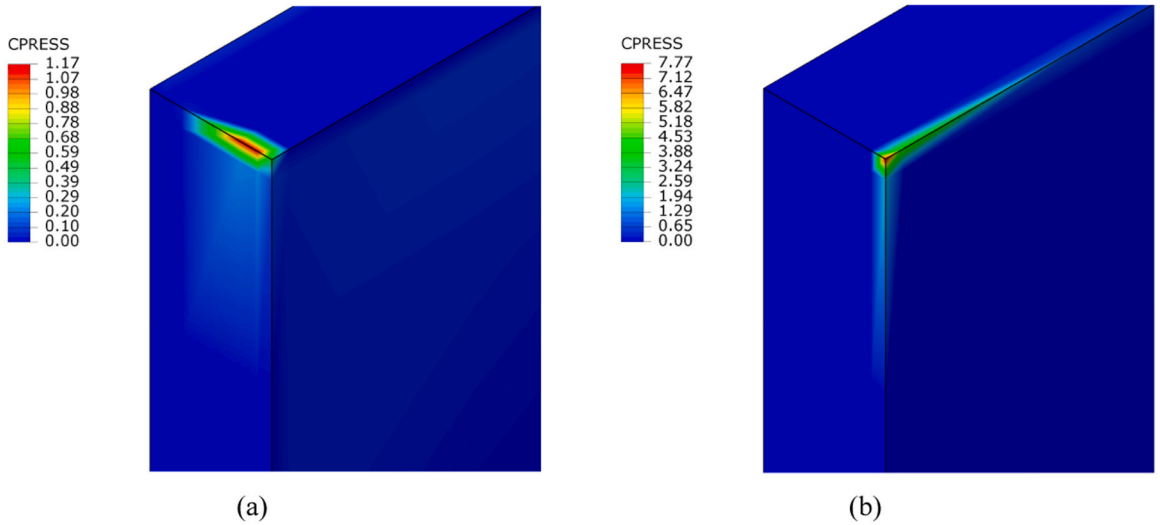

Fig. 17. Contact point on the glass panel as a function of the imposed in-plane lateral displacement (ABAQUS): (a) 27 mm and (b) 45 mm (values in MPa).

Table 9
Effect of glass-frame local contact.

Input property	Input value	Variation	Major observed effect	
Aluminium frame MoE	70,000 MPa	1000 MPa (−99 %)	Maximum load	−0.8 %
		210,000 MPa (+200 %)		+ 4.2 %
Silicone (in-plane) MoE	2 MPa	70,000 MPa (like glass/aluminium)	Maximum load	+ 0.8 %
		140,000 MPa (×2)		+ 0.9 %

without overstressing them, and to optimise further the presented numerical strategy.

6. Local performance assessment

A final attention was paid to the local performance assessment of the examined system.

Despite the rather good agreement obtained with the experimental results for both MREF and MSIMP models, the analysis of local phenomena highlighted possible major consequences and limitations with critical effects for structural safety considerations and assumptions. In particular, it is well recognized that the evaluation of stress peaks in IGUs are of primary importance to verify the possible glass failure under the assigned mechanical loads. In this regard, Fig. 22 shows the principal compressive stress distribution that was numerically obtained in the most stressed glass elements for MREF and MISMP assemblies, when subjected to a maximum imposed in-plane lateral displacement of 45 mm.

Due to the glass-frame contact, the MREF in Fig. 22 (a) shows a compression strut along the diagonal of glass pane, with a stress concentration at the corners, which reminds the schematic mechanisms of Fig. 1. As expected, the maximum principal stress was in fact numerically recorded at the contact point with the frame, and resulted in approximately ≈ 38 MPa in tension and ≈ 32 MPa in compression. It should be noted that the principal tensile stress is perpendicular to the compressive stress along the diagonal, due to the contact mechanism. Most importantly, both these stresses values resulted lower than the reference strength of annealed glass, for which a tensile strength of 45 MPa, and about ten times higher in compression, can be taken into account as characteristic values. Such an outcome well agrees with the results of the experimental test presented in [27], in which no breakage was observed in the glass elements at the maximum imposed displacement of 45 mm. Finally, such an assumption further justifies the use of linear elastic material properties for the present numerical investigations.

For MSIMP, see Fig. 22 (b), the diagonal propagation of stresses that was properly identified in MREF is not clearly detected. Moreover, the

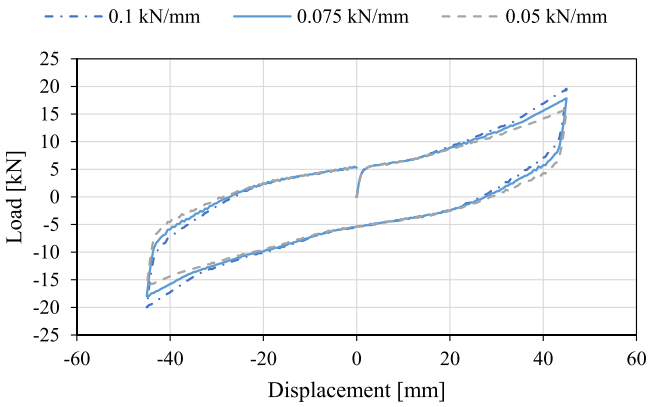

Fig. 20. Effect of glass-to-frame contact stiffness on the cyclic load-displacement response.

Table 10
Effect of rubber pads.

Input property	Input value	Variation	Major observed effect	
PVB MoE	2 MPa	10 MPa (+400 %)	Maximum load	+ 19 %
		50 MPa (+2000 %)		+ 29 %

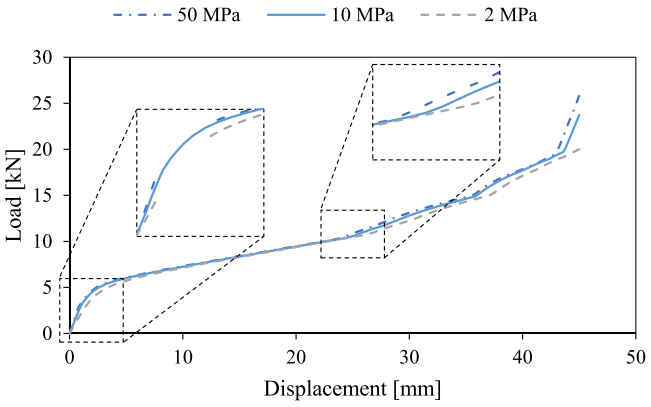

Fig. 21. Effect of rubber pad stiffness (MoE) on the monotonic load-displacement response.

stress concentration is mostly located in the region of setting blocks, and achieves a maximum peak of about ≈ 8 MPa in compression, which is approximately in the order of four times lower than MREF. This distribution and amplitude of stress prediction for glass is the main

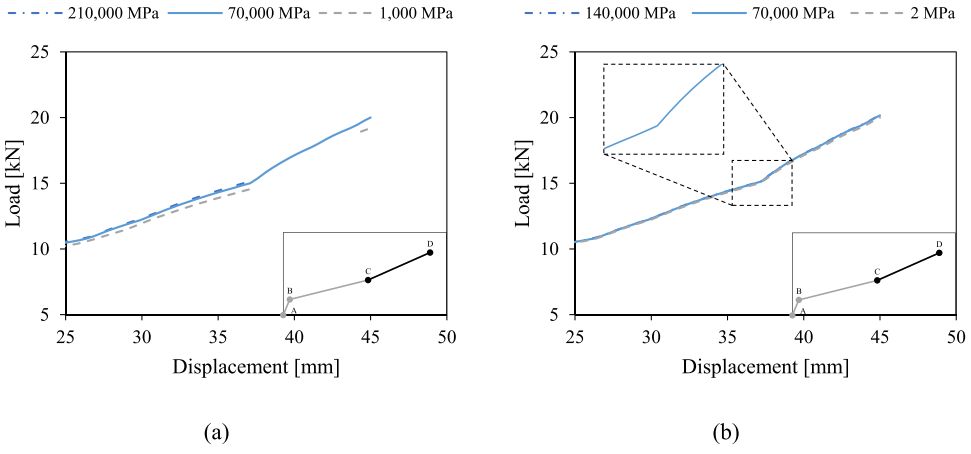

Fig. 19. Effect of (a) frame and (b) glass local stiffness (MoE) on the monotonic load-displacement response.

Table 11
Sensitivity analysis results (MREF model). Sensitivity: x = low; xx= high.

Parameter	Variation	Major observed effect			Sensitivity
Glass-gaskets friction	+ 8.7 % −8.7 %	1st branch (AB)	Strength	+ 5 % −5 %	x
Frame in-plane lateral stiffness	+ 15 % −15 %	2nd branch (BC)	Stiffness	−21 % + 48 %	xx
Glass-frame clearance	−33.3 % + 33.3 %	2nd branch (BC)	Contact displacement	−26 % + 23 %	xx
Glass-frame mechanical interaction (local contact)	−99 % + 2000 %	3rd branch (CD)	Maximum load	−0.8 % + 4.2 %	x
	Like glass/aluminium × 2	3rd branch (CD)	Maximum load	+ 0.8 % + 0.9 %	x
Rubber pad stiffness	+ 400 % + 2000 %	3rd branch (CD)	Maximum load	+ 19 % + 29 %	xx

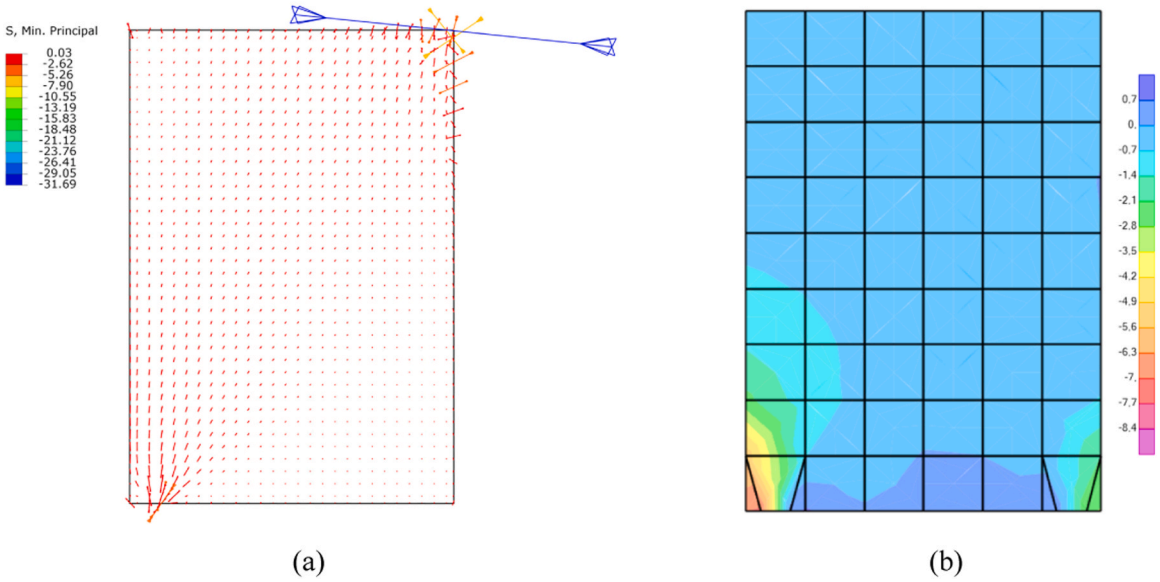

Fig. 22. Compressive principal stress distribution in glass elements for (a) MREF and (B) MSIMP at the maximum imposed displacement of 45 mm (values in MPa).

consequence of MSIMP concept assembly, and derives from the fact that the mechanical interaction between IGUs and frame members is not correctly captured by the simplified numerical model, which is not the case of MREF. In this regard, it is important to note that such an intrinsic limit was also emphasized in [27]. Therefore, the MSIMP assembly looks computationally efficient to predict the global load-displacement response of similar façade systems, but not sufficiently accurate and robust for conservative design considerations at the component level. A more accurate model is necessarily required to capture the local behaviour of glass panels and describe the stress concentration which derives from the imposed in-plane lateral displacements.

Such a result also further highlights that careful consideration should be taken into account in the use of approximate modelling strategies for the structural performance assessment of similar systems, especially in terms of mechanical interaction between IGUs and frame components.

7. Conclusions

Façades are complex and vulnerable building components due to the intrinsic fragility and brittleness of glass. Therefore, specific design and calculation tools are required, especially under extreme conditions. In this paper, the attention was focused on the behaviour of Glass Curtain Walls (GCWs) subjected to a horizontal in-plane seismic action. In particular, the use of two different numerical modelling strategies to evaluate the in-plane seismic performance of a literature glass façade prototype was addressed. The global in-plane lateral performance was rather well captured by both the herein developed refined and simplified numerical assemblies. The global response was described in three branches, detecting for each of them the most influential parameter. In detail:

- the first branch is characterised by a relatively high stiffness, which is mainly governed by the friction between the glass panels and the gaskets;
- the second branch is governed by the lateral stiffness of the bare aluminium frame and shows a marked stiffness decrease, compared to the first branch;
- the third branch is mostly affected by the localised contact between the glass panels and the frame and exhibit an additional increase of in-plane lateral stiffness.

The influence of the aforementioned mechanisms and parameters was quantified through a sensitivity parametric analysis, conducted both on the refined and simplified models. The following parameters were considered:

- Friction between glass and gaskets;
- In-plane lateral stiffness of the aluminium frame;
- Clearance between glass and frame;
- Local stiffness in the mechanical interaction between glass and frame;

- Rubber pad stiffness.

Among others, the parametric analysis allowed to identify the key role of the rubber pads, and in general of "secondary" components, on the complex mechanical interactions that govern the structural behaviour of façades. However, further experimental tests are necessary to investigate the effect of different types of rubber pads and setting blocks. Finally, possible safety risks related to simplified modelling strategies in terms of local performance analysis were highlighted. In detail, a scatter up to 4 times in the predicted compression stress peaks in glass was obtained, confirming the intrinsic limitations of simplified numerical approaches and the need of refined computational strategies for a reliable modelling of the mechanical interaction between glass and frame. In this regard, further efforts are needed for the optimization of refined numerical strategies and the definition of efficient approaches for the description of "secondary" components. At the same time, the use of simplified models to predict the global load-displacement response is still possible, but requires further investigations to establish a reliable correlation between the facade features and the model without the use of full-scale prototype experimental tests.

CRediT authorship contribution statement

Chiara Bedon: Writing – original draft, Supervision, Data curation. **Nicola Cella:** Writing – original draft, Software, Investigation, Formal analysis, Data curation.

Declaration of Competing Interest

The authors declare that they have no known competing financial interests or personal relationships that could have appeared to influence the work reported in this paper.

Data availability

Data will be made available on request.

References

[1] EN 13830:2015 - Curtain walling – Product Standard, Bruxelles, Belgium: European Committee for Standardization (CEN), 2015.
[2] Bedon C, Zhang X, Santos F, Honfi D, Kozłowski M, Arrigoni M, Figuli L, Lange D. Performance of structural glass façades under extreme loads - Design methods, existing research, current issues and trends. Constr Build Mater 2017;163:921–37.
[3] Lee H, Oh M, Seo J, Kim W. Seismic and energy performance evaluation of large-scale curtain walls subjected to displacement control fasteners. Appl Sci 2021;11:6725.
[4] Bedon C, Amadio C. Numerical assessment of vibration control systems for multi-hazard design and mitigation of glass curtain walls. J Build Eng 2018;15:1–13.
[5] Yang Y, Wang P, Wang J, Jin X. Seismic analysis of the hung curtain wall structure in Shanghai Center Tower. Struct Des Tall Spec Build 2010;22(11):847–61.
[6] Memari AM, Behr RA, Kremer PA. Seismic behavior of curtain walls containing insulating glass units. J Archit Eng 2003;9:70–85.
[7] Aiello C. In-plane seismic response of a glazed curtain wall: full-scale laboratory test and non-linear modelling. Proc 7th ECCOMAS Themat Conf Comput Methods Struct Dyn Earthq Eng, Crete, Greece 2019.
[8] Brueggeman JL, Behr RA, Wulfer H, Memari AM, Kremer PA. Dynamic racking performance of an earthquake-isolated curtain wall system. Earthq Spectra 2000;16:735–56.
[9] Bianchi S, Lori G, Hayez V, Overend M, Manara G. Influence of design variables on seismic performance of unitized curtain walls: a parametric experimental study. Glass Struct Eng 2024. https://doi.org/10.1007/s40940-024-00255-2.
[10] Huang B, Chen S, Lu W, Mosalam KD. Seismic demand and experimental evaluation of the nonstructural building curtain wall: a review. Soil Dyn Earthq Eng 2017;100:16–33.
[11] O'Brien WC, Memari AM, Kremer PA, Behr RA. Fragility curves for architectural glass in stick-built glazing systems. Earth Spectra 2012;28:639–65.
[12] Mattei S, Bedon C. Analytical fragility curves for seismic design of glass systems based on cloud analysis. Symmetry 2021;13:1541.
[13] Memari AM, Shirazi A, Kremer PA. Static finite element analysis of architectural glass curtain walls under in-plane loads and corresponding full-scale test. Struct Eng Mech 2007;25(4):365–82.
[14] Memari AM, Shirazi A, Kremer PA, Behr RA. Development of finite-element modeling approach for lateral load analysis of dry-glazed curtain walls. J Archit Eng 2011;17(1). https://doi.org/10.1061/(ASCE)AE.1943-5568.0000027.
[15] Memari AM, Shirazi A, Kremer PA, Behr RA. Seismic vulnerability evaluation of architectural glass in curtain walls. J Civ Eng Archit Res 2014;1(2):110–28.
[16] Caterino N. A simplified analytical approach for assessing non-linear in plane seismic response of stick-built glass curtain walls. Structures 2023;49:281–94.
[17] Sucuoğlu H, Vallabhan CVG. Behaviour of window glass panels during earthquakes. Eng Struct 1997;19(8):685–94.
[18] EN 1998–1:2004 Eurocode 8 - Design of structures for earthquake resistance - Part 1: General rules, seismic actions and rules for buildings, Brusselles, Belgium: European Committee for Standardization (CEN), 2004.
[19] ASCE 7–10, Minimum Design Loads for Buildings and Other Structures, Reston, USA: American Society of Civil Engineers, 2010.
[20] AAMA 501.4–01 - Recommended Static Test Method For Evaluating Curtain Wall And Storefront Systems Subjected To Seismic And Wind Induced Interstory Drifts, Schaumburg, USA: American Architectural Manufacturers Association (AAMA), 2001.
[21] AAMA 501.6–01 - Recommended Dynamic Test Method For Determining The Seismic Drift Causing Glass Fallout From A Wall System, Schaumburg, USA: American Architectural Manufacturers Association (AAMA), 2001.
[22] Jin YZ, Wang XL, Li J, Yang Y. Numerical analysis for seismic response of a super-tall curtain wall structure considering glass stiffness. J Vib Shock 2012;31(8):86–91.
[23] Barnaure M, Voiculescu M. The seismic behaviour of curtain walls: an analysis based on numerical modelling. Math Model Civ Eng 2013;9(4). https://doi.org/10.2478/mmce-2013-0013.
[24] Caterino N, Del Zoppo M, Maddaloni G, Bonati A, Cavanna G, Occhiuzzi A. Seismic assessment and finite element modelling of glazed curtain walls. Struct Eng Mech 2017;61(1):77–90.
[25] Casagrande L, Bonati A, Occhiuzzi A, Caterino N, Auricchio F. Numerical investigation on the seismic dissipation of glazed curtain wall equipped on high-rise buildings. Eng Struct 2019;179:225–45.
[26] Rossetti M, Milardi M, Sansotta S. Seismic evaluation of a curtain wall system for improving the adaptive performance of connecting nonstructural components. In: Sayigh A, editor. Mediterranean architecture and the green-digital transition innovative renewable energy, 2023. Cham: Springer; 2023. https://doi.org/10.1007/978-3-031-33148-0_17.
[27] Aiello C, Caterino N, Maddaloni G, Bonati A, Franco A, Occhiuzzi A. Experimental and numerical investigation of cyclic response of a glass curtain wall for seismic performance assessment. Constr Build Mater 2018;187:596–609.
[28] Simulia. Abaqus Computer Sotfware. Providence, RI, USA: Dassault Systèmes; 2014.
[29] Bedon C, Amadio C. Mechanical analysis and characterization of IGUs with different silicone sealed spacer connections - Part 1: experiments. Glass Struct Eng 2020;5:301–25.
[30] Bedon C, Amadio C. Mechanical analysis and characterization of IGUs with different silicone sealed spacer connections - Part 2: modelling. Glass Struct Eng 2020;5:327–46.
[31] Computers and Structures Inc. SAP2000 - Static and Dynamic Finite Element Analysis of Structures, Berkeley, USA.